Am J Physiol Heart Circ Physiol 304: H398–H405, 2013.
First published December 7, 2012; doi:10.1152/ajpheart.00550.2012.

Endothelial barrier dysfunction in diabetic conduit arteries: a novel method to quantify filtration

Xiao Lu,[1] Virginia H. Huxley,[2] and Ghassan S. Kassab[1,3]

[1]*Biomedical Engineering, Indiana University-Purdue University, Indianapolis, Indiana;* [2]*Department of Medical Pharmacology and Physiology, University of Missouri School of Medicine, Columbia, Missouri; and* [3]*Department of Cellular and Integrative Physiology, Department of Surgery, and Indiana Center for Vascular Biology and Medicine, Indiana University-Purdue University, Indianapolis, Indiana*

Submitted 19 July 2012; accepted in final form 4 December 2012

Lu X, Huxley VH, Kassab GS. Endothelial barrier dysfunction in diabetic conduit arteries: a novel method to quantify filtration. *Am J Physiol Heart Circ Physiol* 304: H398–H405, 2013. First published December 7, 2012; doi:10.1152/ajpheart.00550.2012.—The endothelial barrier plays an important role in atherosclerosis, hyperglycemia, and hypercholesterolemia. In the present study, an accurate, reproducible, and user-friendly method was used to further understand endothelial barrier function of conduit arteries. An isovolumic method was used to measure the hydraulic conductivity (L_p) of the intact vessel wall and medial-adventitial layer. Normal arterial segments with diameters from 0.2 to 5.5 mm were used to validate the method, and femoral arteries of diabetic rats were studied as an example of pathological specimens. Various arterial segments confirmed that the volume flux of water per unit surface area was linearly related to intraluminal pressure, as confirmed in microvessels. L_p of the intact wall varied from 3.5 to 22.1 $\times$ 10^{-7} cm·s^{-1}·cmH_2O^{-1} over the pressure range of 7–180 mmHg. Over the same pressure range, L_p of the endothelial barrier changed from 4.4 to 25.1 $\times$ 10^{-7} cm·s^{-1}·cmH_2O^{-1}. During perfusion with albumin-free solution, L_p of rat femoral arteries increased from 6.1 to 13.2 $\times$ 10^{-7} cm·s^{-1}·cmH_2O^{-1} over the pressure range of 10–180 mmHg. Hyperglycemia increased L_p of the femoral artery in diabetic rats from 2.9 to 5.5 $\times$ 10^{-7} cm·s^{-1}·cmH_2O^{-1} over the pressure range of 20–135 mmHg. In conclusion, the L_p of a conduit artery can be accurately and reproducibly measured using a novel isovolumic method, which in diabetic rats is hyperpermeable. This is likely due to disruption of the endothelial glycocalyx.

hydraulic permeability; endothelial barrier; conduit vessel; glycocalyx

UNDER PHYSIOLOGICAL CONDITIONS, the endothelial barrier plays an important role in homeostasis and regulates the movement of fluid and solutes across the vessel wall (9, 28, 34, 46, 47). The ease of fluid movement across the endothelial barrier is described by the hydraulic conductivity (L_p), and changes in L_p likely provide an assessment of barrier exchange function for water-soluble solutes (27). Endothelial barrier dysfunction, which has been implicated in the pathogenesis of diabetes and atherosclerosis (6, 10–12, 19, 29–33, 35–36, 43, 47), is typically characterized by endothelial hyperpermeability to solutes and water (9, 12).

The majority of observations and theoretical analysis of the endothelial barrier has focused on the microvasculature, given that nutrient and waste product exchange between blood and tissue is the major function of this portion of the vascular bed (28). Hyperglycemia is a known culprit of microvascular hyperpermeability (19, 36) and is thought to damage the glycocalyx overlaying the endothelium. Thus, hyperglycemia contributes to increased solute and volume flux (J_v) in the microvessels (11, 31, 32, 43). Endothelial glycocalyx dysfunction has also been implicated in the atherothrombotic process (33).

The risk of atherosclerosis is higher in conduit arteries with the presence of hypertension, hypercholesterolemia, and hyperglycemia (38). Endothelial cell (EC) dysfunction, including a decrease in endothelial nitric oxide production and an increase in oxidative stress, inflammation, adhesive molecular activation, and endothelial barrier dysfunction, have been identified as landmark features of atherogenesis (10, 33, 47). Therefore, an understanding of endothelial barrier function in conduit arteries is essential to understanding the pathogenesis of atherosclerosis.

Endothelial barrier function in conduit arteries also affects the delivery of substrates and regulators of vascular smooth muscle function, i.e., nutrients must pass through the glycocalyx and ECs to reach target vascular cells. The vessel barrier to volume and solutes is a composite structure consisting of ECs with the glycocalyx at the surface, the basement membrane below, and surrounding contractile cells (pericytes in the capillaries to vascular smooth muscle cells in other vessel types). Thus, the resistance to flux offered by the endothelium is the sum of serial glycocalyx and EC resistances to solutes (e.g., plasma proteins) and solution (water) (13). L_p is an index of the barrier leakiness to water (12).

In this study, we introduce an isovolumic method to quantify L_p (J_v of water) of the vascular wall (21). L_p of the endothelial barrier of arteries was calculated by measuring the L_p of intact and endothelium-denuded vessels, respectively. Since atherosclerosis occurs more frequently in diabetes, we also tested the hypothesis that conduit vessel L_p is higher in type 2 diabetes mellitus (DM2).

MATERIALS AND METHODS

Animal experiments were performed in accordance with the guidelines of the Institute of Laboratory Animal Research Guide, Public Health Service Policy, and Animal Welfare Act. Protocols were approved by the Institutional Animal Care and Use Committee of the Indiana University School of Medicine.

Animal and tissue preparation. To establish the method, 12 Duroc swine (both sexes) at 5 mo of age weighing 51 ± 9 kg were obtained from Michigan State University and housed at the Indiana University School of Medicine facilities (Laboratory Animal Resource Center). In conjunction, 18 male Wistar rats were obtained at 12 wk of age with a body weight of 386 ± 18 g (Charles River; Laboratories International). To test the hypothesis that diabetes induces an increase

Address for reprint requests and other correspondence: G. S. Kassab, Dept. of Biomedical Engineering, Indiana Univ.-Purdue Univ., Indianapolis, IN 46202 (e-mail: gkassab@iupui.edu).

in L_p of a conduit artery, six male Zucker diabetic fatty (ZDF) rats and six male Zucker lean (ZL) rats were obatined at 18 wk of age with a body weight of 439 ± 26 g (ZDF) and 413 ± 22 g (ZL) (Charles River; Laboratories International) and used in the study. The degree of hyperlycemia in ZDF rats has been verifed in our previous study (22). All animals were acclimated to the facility for ~1 wk before the start of the study.

On the day of experimentation, pigs were anesthetized with telazol (10 mg/kg), ketamine (5 mg/kg) and xylazine (5 mg/kg), maintained with isoflurane (1–2%), and euthanized by overanesthesia with pentobarbital sodium (150 mg/kg iv). Rats were first anesthetized with pentobarbital sodium (50 mg/kg ip) and euthanized by overanesthesia with pentobarbital sodium (150 mg/kg ip). Swine carotid arteries (n = 9) and right coronary arteries (n = 8) were harvested. Either aortas (n = 8), common femoral arteries (n = 10), or mesenteric arteries (n = 9) of Wistar rats were excised. The femoral arteries of either ZDF (n = 9) or ZL (n = 7) rats were harvested similarly. All arterial segments were immediately placed in ice-cold physiological saline solution [PSS; containing (in mmol/l) 119 NaCl, 4.6 KCl, 0.15 $NaHPO_4$, 0.4 KH_2PO_4, 20 HEPES acid, 1 $NaHCO_3$, 1 $MgSO_4$, 1.2 $CaCl_2$, and 5.5 glucose; pH 7.4]. Each artery was carefully cleaned from the adjacent tissue with the aid of a stereomicroscope. The artery was allowed to warm up to room temperature (22°C) slowly over a 10- to 15-min period, and the branches on the artery were ligated. The arterial segment (length varied from 8 to 15 folds of the diameter) was transferred to the chamber of isovolumic system, and the segment was cannulated on connectors and tied with 8-0 suture twice to avoid leaks, which were detected using blue dextran (dextran molecular mass: ~2,000 kDa with blue color, no. D5751-1G, Sigma-Aldrich). The artery was then warmed to 37°C over a 20- to 25-min period and equilibrated for 40 min at a transmural pressure of ~10 mmHg before the start of the experimental protocol.

Volume of filteration across the vessel wall. Our system consisted of a chamber, a solid-state pressure transducer (SPR-524, Microtip catherter transducer, Millar Instruments), a four-way connector, a gas-tight microsyringe (National Scientific) operated by a linear pump (UltraMicroPump III, World Precision Instruments) and a controller (Micro 4, World Precision Instruments), and a screw-secure clamp assembled together, as shown in Fig. 1. Free fatty acid BSA was obtained from Sigma (A4378) and dialyzed to obtain γ-globulin-free albumin (15). PSS or PSS-BSA (10 mg/ml) was aerated with mixed gas (room air with 5% CO_2) and filled the chamber (superfusate) and tubes (perfusate). A charge-coupled device camera on a microscope transfered the image of the vessel to a computer, which digitized the external diameter of the nontransparent vessel wall while the internal diameter was calculated using the incompressibility assumption (21). The vessel segment was pressurized to the desired pressure. The clamp was closed until the vessel tone was stable, which typically occurred in 10–20 min. The hydrostatic pressure is the driving force for the "transport" of J_v across the vessel wall, which results in a loss of internal fluid volume and, consquently, a gradual decrease in transluminal pressure. The gas-tight microsyringe was used to inject an equal volume of PSS in the lumen of the vessel to maintain constant pressure (variation less than ±0.2 mmHg/min). At constant tone, the injection volume rate (called the compensatory rate) provides J_v of water across the vessel wall. In addition to the filtration of the vessel wall, a small leak may exist despite the gas-tight connections that may be too small to be detected by blue dextran. To evaluate the small leak of the system, an impermeable silicone rubber tube (instead of the blood vessel) was mounted in the chamber, and the leak rate was measured at various pressures. Thus, the J_v of water across the vessel wall was equal to the compensatory rate of the blood vessel minus the systemic leak rate at equivalent pressure. A baseline vessel tone is important to establish an accurate filtration. In our experiments, a vasoconstriction or vasorelaxation resulted in either a sharp increase or decrease in pressure, respectively. Vasoconstriction caused an increase in pressure, which was in contrast to the filtration-induced decrease in pressure. Vasorelaxation caused a sharp decrease in pressure, which required a much larger compensatory rate (10^{-3}-10^{-1} cm^3/min), in contrast to ~10^{-4} cm^3/min for filtration. We differentiated between filtration and leakage (wall damage) by either the extent of the compensatory rate or blue dextran. Leakage due to damage of the vessel wall resulted in a large compensatory rate (>3 × 10^{-2} cm^3/min) or blue dextran out of the vessel wall. Such vessels were excluded from analysis (1 of 10 vessels).

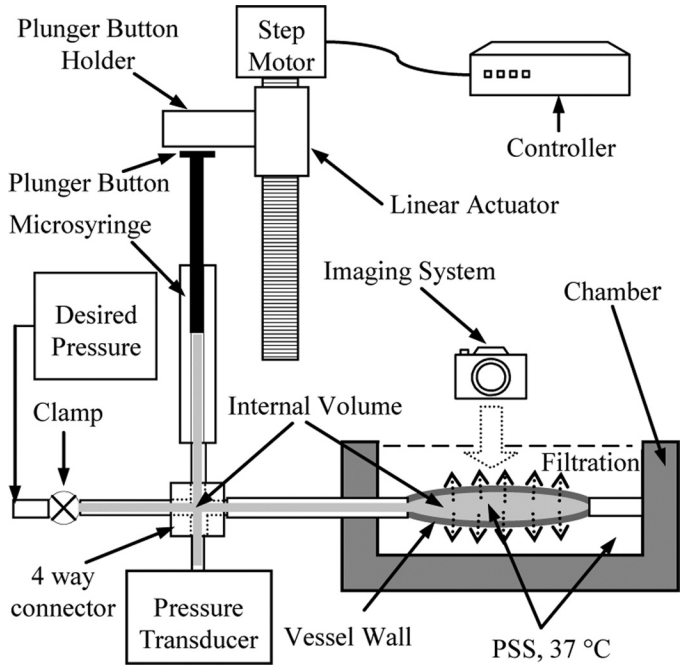

Fig. 1. Schematic of the isovolumic system used to measure the volume flux (J_v) of water across the blood vessel wall. Dimensional tracking software accounted for the occupied pixels of a vessel image, and a data-acquisition system recorded the diameter of the vessel continuously. PSS, physiological saline solution.

To compare the isovolumic method with the current method to measure the J_v of water, a parallel capillary (a stiff, thick-walled plastic tube with an inner diameter of 0.0508 cm) was connected to the microsyringe-transduser unit in the isovolumic system. An air bubble was introduced into the capillary, and the travel velocity of the bubble was measured during vessel wall filtration under a given transmural pressure. The J_v measured by the air bubble velocity (J_v^{air}) was compared with that of the isovolumic method (J_v^{iso}) to determine the agreement between the two methods. The two methods were also verified by observing the air bubble movement during microsyringe compensation when the vessel segment was simultaneously exposed to the capillary (air bubble velocity method) and microsyringe (isovolumic method). The air bubble did not move when the microsyringe compensation was equal to the J_v water across the vessel wall.

Starling's law. Fluid movement in the microvessel is described by Starling's law as follows (12, 44):

$$J_v = L_p S(\Delta P - \sigma \Delta \pi) \quad (1)$$

where J_v is the volume flux across the vessel wall (×10^{-6} cm^3/s), L_p is the hydraulic conductivity (in $cm \cdot s^{-1} \cdot cmH_2O^{-1}$) of the intact vessel wall, and S is the luminal surface area (×10^{-2} cm^2), which was calculated using an incompressibility assumption of the vessel wall. ΔP and $\Delta \pi$ are the hydraulic and oncotic pressure differences between the vascular and tissue space, respectively, and σ is the osmotic reflection coefficient (unitless). In the present study, we provided the same physiological solution internal and external to the vessel. Therefore, $\Delta \pi$ was equal to zero. Given the layered structure of the vessel

wall, total $\Delta\pi = 0$ does not guarantee equality of osmolarity at each filtration barrier, albeit the difference of osmolarity at each layer should be small when the total equals 0. Therefore, we neglected the difference of $\Delta\pi$ at each barrier of the blood vessel wall. For conduit arteries, the media and adventitia are thicker (over 10 times the wall thickness of arterioles) than those in the microvessel and form a significant barrier to the J_v of water across the wall. We used L_p^E and L_p^{MA} to indicate endothelial and medial-adventitial L_p, respectively. L_p for the intact vessel may be subdivided between the series components of L_p^E and L_p^{MA} by the following equation (13, 45, 49):

$$\frac{1}{L_P} = \frac{1}{L_P^E} + \frac{1}{L_P^{MA}} \quad (2)$$

or

$$\frac{1}{L_P^E} = \frac{1}{L_P} - \frac{1}{L_P^{MA}} \quad (3)$$

Hence, L_p^E can be calculated from intact L_p and L_p^{MA}.

The endothelial barrier presents a multicomponent barrier for J_v and solute flux, having both a glycocalyx in series with the endothelium and the associated basement membrane. The hydraulic resistance of the endothelial barrier (R^E) is the sum of the hydraulic resistance of the glycocalyx (R^{Glyco}) as well as the EC and basement membrane (R^{EC}), as follows:

$$R^E = R^{Glyco} + R^{EC} \quad (4)$$

Since the product of hydraulic resistance and conductivity is equal to 1, we can obtain the following:

$$1/L^E = 1/L^{Glyco} + 1/L^{EC} \quad (5)$$

Experimental protocol. Systemic leak rates were measured at pressures ranging from 0 to 180 mmHg before the vessel segment was mounted in the chamber. The perfusate and bath solution (superfusate) were PSS-BSA. After the vessel segment was pressurized at 10 mmHg and the temperature of the chamber was increased gradually from 22 to 37°C, a 40-min equilibration period was initiated. At this point, the compensatory rates and diameters of the vessel segment were measured at various pressures. In the arteries of diabetic rats, the segments were incubated with the myosin light chain kinase (MLCK) inhibitor 1-(5-iodonaphthalene-1-sulfonyl)homopiperazine (ML-7; 10–7 mol/l, Sigma) for 10 min (51). In one set of experiments, the contribution of the glycocalyx (R^{Glyco}) was assessed by replacing PSS-BSA with PSS (both perfusate and superfusate) (17, 37), which was then infused into the segment for 15 min at 10 mmHg. Compensatory rates of the vessel segment in PSS were measured at various pressures. Vessel segments were disconnected from connectors, and the endothelium was denuded with a wire (diameter range of 0.25–5.2 mm) using a previously validated protocol (23) to determine the contribution of R^{EC}. Vessel segments were then reconnected to the connectors by the same standardized procedure as the intact vessel, and compensatory rates of the vessel segments in PSS-BSA were measured at various pressures. Vessel segments were then contracted using PSS-BSA with 60 mM KCl. At the vessel contraction induced by 60 mmol/l KCl, the compensatory rates of the vessel segments were measured over a range of pressures. PSS-BSA with 60 mM KCl was drained, and the vessel segments were rinsed three times using PSS-BSA. Ca^{2+}-free PSS-BSA was introduced in the chamber to relax the vessel segments, and compensatory rates were measured one final time over the same pressure range during a steady relaxation period.

Data analysis and statistics. Data are expressed as means ± SD unless otherwise stated. The relation of J_v^{iso} and J_v^{air} was expressed as follows: $J_v^{iso} = \alpha J_v^{air} + \beta$, where α and β are empirical constants that were determined with a linear least-squares fit along with the corresponding correlation coefficient (R^2). In a Bland-Altman scatter diagram (4), we plotted the ratio differences (to indicate the percentage of the difference) between the two measurements $[(J_v^{air} - J_v^{iso})/J_v^{air}]$ against their means $[(J_v^{air} + J_v^{iso})/2]$. In the scatter diagram, the precision and bias of the method were quantified. The relationship of $J_v(J_v/S)$ to pressure was analyzed using a linear least-squares fit. Student's *t*-test was used to detect differences between pairwise groups of L_p. For all analyses, *P* values of <0.05 were used to indicate statistical significance.

RESULTS

The femoral arteries of Wistar rats were used to validate the methodology for the determination of L_p. Figure 2*A* shows the rationale for determining the J_v of a segment of a femoral artery at physiological pressure. When the clamp was closed, various compensatory rates were applied to determine the correct flow to maintain a constant pressure in the system. For this vessel, a rate of 140×10^{-6} cm^3/min was found to maintain the pressure constant at 82.9 mmHg (where 130×10^{-6} cm^3/min was too low and 190×10^{-6} cm^3/min was too high). The diameter of the segment did not change during the adjustment period of the compensatory rate (Fig. 2*B*). Constant diameter is the signature of a stabilized vessel tone. This procedure was carried out for each vessel segment. The repeatability of the isovolumic method was verified by five repeated measurements under the same conditions, and the difference of L_p over the five measurements was $<5\%$.

Figure 3*A* shows the correlation of J_v based on isovolumic and air bubble methods. The linear least-squares fit showed a highly significant correlation ($R^2 = 0.988$) corresponding nearly to an identity line. A Bland-Altman plot is shown in Fig. 3*B* (average of two measurements vs. ratio difference), and the data scattered randomly within 2 SD of the mean of the ratio difference (i.e., no significant bias), which indicates the percentage of the variation. The root mean square was 12.3% of the mean value of the two methods. This analysis shows that the isovolumic method is an accurate surrogate of J_v measured using the air bubble method, which has been a classic method (1, 7, 45, 49) for the assessment of filtration across the walls of large vessels. The movement of the air bubble in the capillary was $<0.15\%$/min when the microsyringe in the isovolumic system was used to compensate for filtration.

Figure 4*A* shows the system leak rates and filtration compensatory rates of femoral arteries of Wistar rats for the intact endothelium perfused with PSS-BSA (1% BSA). The system

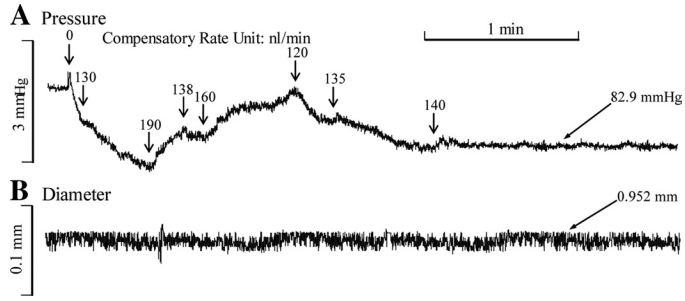

Fig. 2. Sample recordings of pressure and diameter. *A*: pressure variation. When the compensatory rate was inadequate, pressure decreased. When the compensatory rate overshot, pressure increased. When the compensatory rate was equal to the filtration rate, pressure remained constant. The criteria were to maintain constant pressure for at least 2 min. *B*: diameter tracking showing constant diameter.

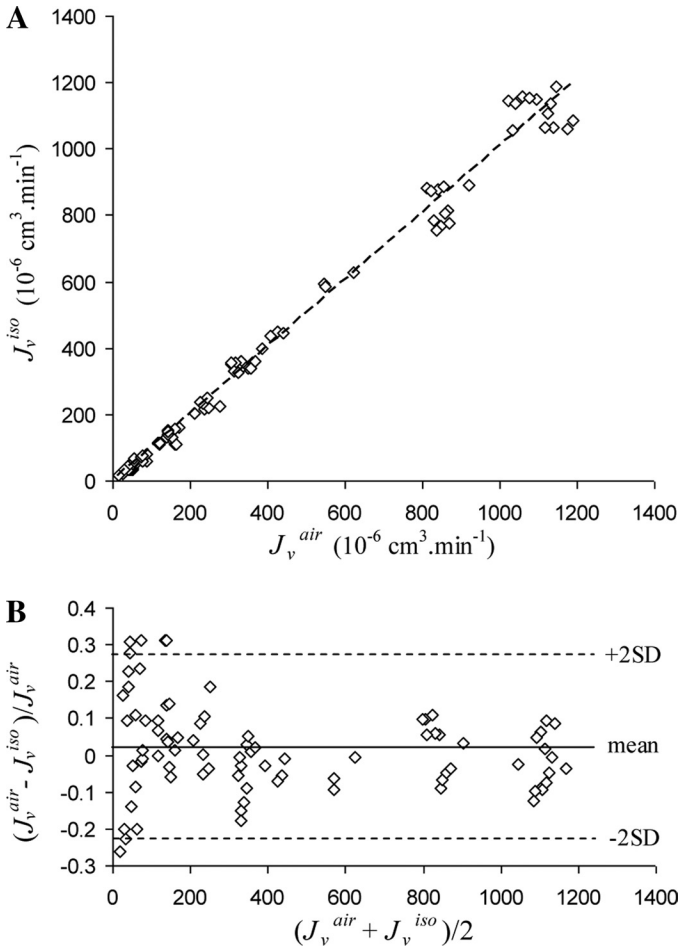

Fig. 3. Comparison of the isovolumic method with air bubble movement in the capillary technique. *A*: linear regression was expressed as follows: $J_v^{iso} = 1.008\ J_v^{air} + 3.3417$, where J_v^{iso} is J_v measured using the isovolumic method and J_v^{air} is J_v measured using air bubble movement method ($R^2 = 0.9881$). *B*: Bland-Altman plot of the difference of J_v in the two methods versus the mean of J_v obtained by the two methods. The mean ± SD for the data was 0.018 ± 0.123. The *top* and *bottom* dotted lines represent the mean + 2SD (0.264) and mean − 2SD (−0.228), respectively.

leakage was much smaller than the compensatory rate of filtration of the rat femoral arteries. The smallest compensatory rate of the system used was 1.33×10^{-6} cm^3/min. J_v of water was determined as the difference of the compensatory rate and leakage rate and normalized by surface area of the vessel wall (J_v/S). We evaluated L_p of arteries in diameters between ~0.3 and ~5 mm and wall thickness from ~0.02 to 0.2 mm (Table 1). The general trends were that vessels with thinner walls possessed higher L_p^{MA} and vessels with larger diameters have lower L_p^E. Figure 4*B* shows the linear regression of J_v/S and pressure of conduit arteries of different species and anatomic locations with an intact endothelium during perfusion with 1% BSA in PSS. The rat aorta had the least J_v (smallest slope), while the rat mesenteric arteries were the leakiest (largest slope) for the set of arteries studied.

L_p and L_p^{MA} were measured, and L_p^E was computed according to *Eq. 5* (Table 1). Generally, L_p^E was inversely related with vessel diameter such that smaller vessels were leakier than larger vessels. L_p^{MA} decreased with the increase in wall thickness consistent with a thicker wall, offering a greater resistance to filtration.

Figure 5 shows the relation of J_v/S and pressure of Wistar rat femoral arteries. The relationship was found to be linear (Fig. 5*A*), consistent with the Starling relationship (*Eq. 1*), with a slope equal to L_p for the vessel segment (Fig. 5*B*). Figure 5 also demonstrates that L_p increased after the removal of protein from the perfusate and that L_p increased further after denudation. After removal of the endothelium, changes in vascular smooth muscle tone (contraction or relaxation) did not influence L_p^{MA}. Although vessel wall thickness may affect vessel wall L_p, the wall thickness of femoral arteries of rats did not change significantly during vascular reactivity in the isovolumic state.

To evaluate whether an atherogenic risk factor, such as diabetes, is accompanied by changes in fluid exchange, the L_p of femoral arteries from a rat model of diabetes was evaluated

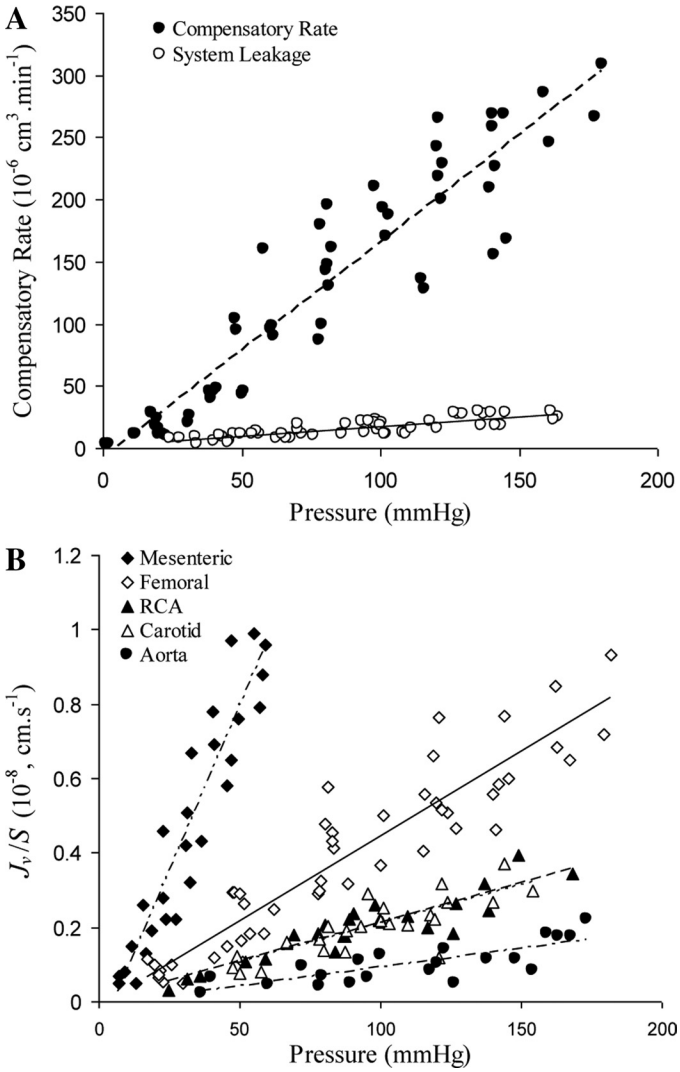

Fig. 4. Evaluation of J_v using the isovolumic system. *A*: the leak rate of the isovolumic system and compensatory rate of femoral arteries of Wistar rats to maintain constant pressure while the endothelium was intact in PSS with 1% BSA. *B*: the relationship between the J_v of water per unit area (J_v/S) and pressures was linear in various arteries. ◆, Rat mesenteric artery; ◇, rat femoral artery; ▲, swine right coronary artery (RCA); △, swine carotid artery; ●, rat aorta.

Table 1. *L_p of the intact wall, L_p^{MA}, and L_p^E in various arterial segments as well as diameters and wall thickness of the arterial segments*

	Number of Segments	L_p, $\times 10^{-7}$ cm·s^{-1}·cmH$_2$O^{-1}	L_p^{MA}, $\times 10^{-7}$ cm·s^{-1}·cmH$_2$O^{-1}	L_p^E, $\times 10^{-7}$ cm·s^{-1}·cmH$_2$O^{-1}	Diameter, $\times 10^{-4}$ cm	Wall Thickness, $\times 10^{-4}$ cm
Rat mesenteric artery	9	22.1 ± 4.5	182.2 ± 45.3	25.1 ± 4.7	286 ± 21	19 ± 3
Rat femoral artery	10	6.1 ± 2.1	32.9 ± 13.1	7.5 ± 2.3	1090 ± 120	52 ± 7
Rat aorta	8	1.3 ± 0.2	16.5 ± 5.3	4.1 ± 0.4	2840 ± 250	110 ± 25
Swine coronary artery	8	3.8 ± 0.9	19.6 ± 3.6	4.8 ± 1.2	3210 ± 340	180 ± 29
Swine carotid artery	9	3.5 ± 0.8	17.8 ± 5.6	4.4 ± 1.5	5260 ± 590	230 ± 46

Values are means ± SD. L_p, hydraulic conductivity; L_p^{MA}, medial-adventitial L_p; L_p^E, endothelial L_p.

(Fig. 6). As demonstrated in vessels from normal animals (Fig. 5*A*), the relationship between J_v/S and pressure remained linear (Fig. 6*A*) during perfusion with protein-containing PSS. L_p of femoral arteries from ZDF rats, however, was significantly higher than that of the control group ($P < 0.05$). To determine whether the change in L_p was simply a consequence of passive alteration of the anatomic structure of the vessels or a consequence of altered endothelial metabolism, L_p was measured in vessels from both groups after inhibition of MLCK with ML-7 (10^{-6} M) (51). After MLCK inhibition, the L_p of both ZDF and ZL femoral arteries did not changed significantly ($P > 0.05$), and the L_p of ZDF arteries remained higher than that of arteries from ZL rats ($P < 0.05$). When BSA was removed from the perfusate, there was no significant change in L_p of ZDF rats, whereas L_p of the arteries from ZL rats increased. Once in protein-free conditions, the difference in L_p between arteries of ZDF and ZL rats was abolished. After the endothelium was denuded in these vessels, the L_p of both ZDF and ZL vessel

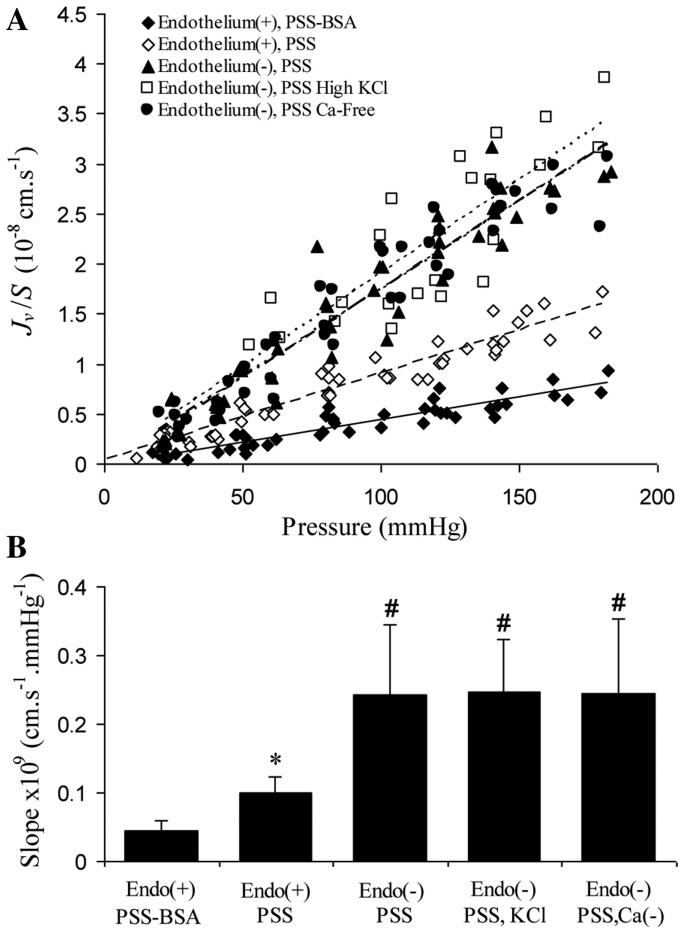

Fig. 5. Validation of the isovolumic method. *A*: the relationship of J_v/S and pressure was linear in femoral arterial segments of Wistar rats under various conditions. ◆, intact endothelium in PSS with 1% BSA; ◇, intact endothelium in PSS without BSA; ▲, denuded endothelium in PSS without BSA; □, denuded endothelium in PSS without BSA at a high concentration of KCl (60 mM); ●, denuded endothelium in PSS without BSA at a zero concentration of Ca^{2+} and a high concentration of EGTA (3 mM). *B*: slopes of the various serial scatter points in *A*, which indicate hydraulic conductivity (L_p) under the various conditions. Endo(+), intact endothelium; PSS-BSA, PSS with 1% BSA; Endo(−), denuded endothelium; KCl, 60 mM KCl in PSS; Ca(−), Ca^{2+}-free PSS with EGTA at 3 mM. *$P < 0.05$ vs. Endo(+) vessels in PSS-BSA; #$P < 0.05$ vs. Endo(+) vessels in PSS.

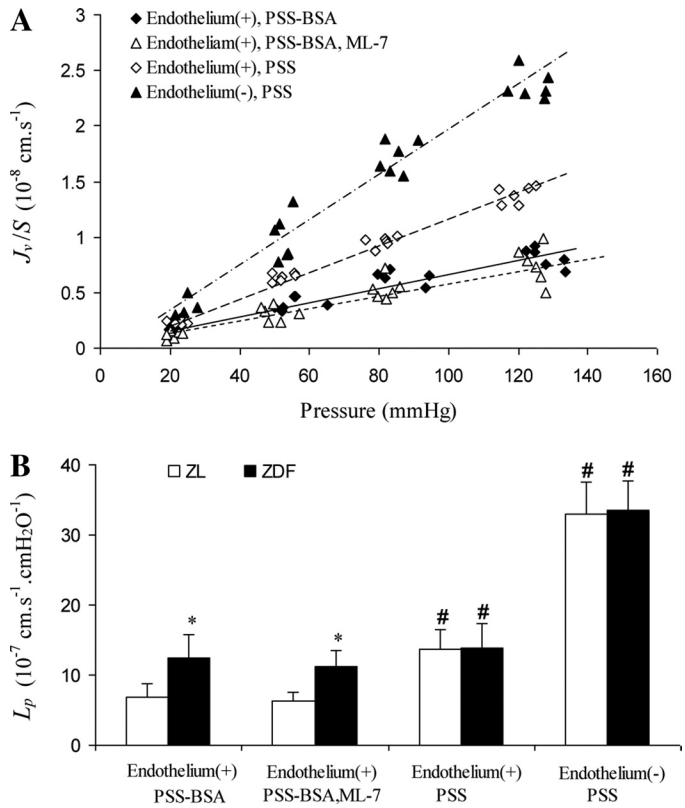

Fig. 6. L_p of femoral arteries of Zucker diabetic fatty (ZDF) and Zucker lean (ZL) rats. *A*: the relationship of J_v/S and pressure was linear. ◆, intact endothelium in PSS with 1% BSA; △, intact endothelium in PSS with 1% BSA with administration of ML-7 (10^{-6} M); ◇, intact endothelium in PSS without BSA; ▲, denuded endothelium in PSS without BSA. *B*: L_p of femoral arteries under various conditions. *B*: hydraulic conductivity of femoral arteries of ZL and ZDF rats at various conditions. Endothelium(+), intact endothelium; PSS-BSA, PSS with 1% BSA; Endothelium(−), denuded endothelium; *$P < 0.05$ vs. Endothelium(+) vessels of ZL rats in PSS-BSA; #$P < 0.05$ vs. Endothelium(+) vessels of ZDF rats in PSS-BSA with ML-7.

walls (L_p^{MA}) increased substantially ($P < 0.05$), and the lack of difference between vessels from ZDF and ZL rats persisted.

DISCUSSION

We developed a new isovolumic technique to measure the L_p of conduit arteries. We found that L_p ranged between 3.5 and 22.1 $\times$ 10^{-7} cm·s^{-1}·cmH$_2$O^{-1} (~7–180 mmHg) in vessels with diameters between 0.28 and 5.3 mm having wall thicknesses between 19 and 230 μm. Using the approach that the barrier to J_v of the conduit vessel is the sum of resistors in series and using approaches to remove each resistor, we found that L_p^E was similar to conduit arteries of different species (rat and pig; 4.1–7.5 $\times$ 10^{-7} cm·s^{-1}·cmH$_2$O^{-1}). L_p^E became significantly larger, however, with decreasing vessel size within a species (25.1 $\times$ 10^{-7} cm·s^{-1}·cmH$_2$O^{-1} in the rat mesenteric artery). L_p^{MA} was dictated largely by the wall thickness, where the thinner the wall, the larger L_p^{MA}. Given that vascular dysfunction (including loss of barrier function) is a feature of DM2, we used the new method to assess the hypothesis that exchange (as assessed from measures of L_p) in the conduit vessel wall is higher in vessels of DM2 relative to sex and age-matched controls. Indeed, we found that L_p values of femoral arteries from an animal model of DM2 were approximately twofold higher (increased from 6.8 ± 2.0 to 12.5 ± 3.4 $\times$ 10^{-7} cm·s^{-1}·cmH$_2$O^{-1}).

Vascular ECs form a semipermeable barrier between blood and tissue to regulate the exchange of fluid, electrolytes, and proteins (3, 13, 15, 42, 51). In the microvasculature, it is well established that endothelial barrier function depends on the glycocalyx at the EC-blood interface, cell-cell junctions (tight and adhesion junctions), and protein transport across the EC (2, 5, 8, 14, 16, 17, 20, 26, 39–41, 48, 50, 52). In microvessels, several studies have shown that L_p of the endothelial barrier is highly related to glycocalyx structure and cell-cell junction integrity (2, 8, 16, 17, 20, 39, 41). Dysfunction of this barrier is associated with multiple acute and chronic disease states, including inflammation, diabetes, traumatic or thermal injury, and tumorigenesis. In the microcirculation, endothelial barrier dysfunction results in tissue edema and organ dysfunction. Recent studies have verified that endothelial barrier dysfunction is also a risk factor for atherosclerosis, a condition that is known to occur primarily in conduit arteries and results in stenosis and possible distal ischemia. In the present study, we introduced and validated a novel method to evaluate endothelial barrier function in vessels ranging from microvessels to macrovessels.

In the 1920s, Landis (18) quantified the filtration of fluid from a single microvessel by measuring the movement of dye in capillaries from a microinjector using a microscope. In later years, additional methods were developed to quantify L_p, including tracking the movement of markers such as red blood cells (24), air bubbles (49), or a silicone oil drop (9, 45). L_p was computed from the change of volume, which was directly proportional to the velocity of the markers, i.e., the movement of markers is indicative of the J_v of water across the vessel wall.

The principle behind the isovolumic method used in this work is that the pressure remains constant in a sealed container when temperature is constant. Any "leak" (filtration or system leaks) will result in a decrease of the pressure in isovolumic conditions and the compensation of an equivalent volume will prevent a decrease in the pressure, i.e., maintain constant pressure. Therefore, the compensatory volume rate to maintain constant pressure is equal to the filtration rate of the vessel plus the system leak rate. The systemic leak rate is too small to detect by the blue dextran used to find tiny branches or damage of blood vessel wall. We used an impermeable silicone tube instead of a blood vessel to measure system leakage. The compensatory volume rate, as in the marker movement methods, can be positive or negative to compensate for leak or absorption, respectively. In our isovolumic system, the J_v of water across the blood vessel wall is the major source of the leak. The compensatory volume rate minus the system leak rate is equal to the J_v of water across the vessel wall. The isovolumic method was also compared with the air bubble technique in capillaries as the gold standard to evaluate L_p of the vessel wall (1, 7, 45, 49). The two methods were in good agreement and can be used interchangeably (Fig. 3). The isovolumic method is an alternative approach to using pressure instead of marker tracking, which is more accurate and lends itself to automation without the need for a microscope.

The isovolumic method eliminates the need for the measurement of a moving air bubble or other motion markers. Transluminal pressure directly indicates hydraulic filtration. The compensatory rate to maintain the pressure constant quantifies the hydraulic filtration. Therefore, the sensitivity of the isovolumic method depends on the precision of microsyringe volume compensation and pressure measurement. Currently, the determination of compensatory rate is done manually, which needs to be automated for future refinement of the system. Similar to other in vitro measurements of filtration, the leak from ligature is a concern for the isovolumic method. We used a standardized procedure for the connection of vessels to prevent the leak from ligatures. We used a Tygon tube directly connected with a blood vessel, since the Tygon tube possesses some elasticity to facilitate a better seal. We chose various Tygon tubes to match the respective diameters of blood vessels, e.g., a heating-pulling method was used to make a different tip diameter of the tubes from 0.25 to 5.2 mm. In addition, four ligatures were tied on each side of the vessel to minimize any possible leaks. In practice, the procedure is very reproducible for connection and reconnection.

Since the media and adventitia are relatively thin in microvessels (small resistance to J_v), the endothelial barrier is the major resistance of the J_v of water. Since the media and adventitia of conduit arteries are much thicker (over 10-fold larger than microvessels), the resistance of media and adventitia to J_v is not negligible in intact arteries, i.e., the media and adventitia also serve as barrier to prevent fluid flow across the vessel wall. Since the endothelium can be mechanically removed without major damage to the medial layer of a conduit artery (23), the permeability of the media and adventitia of a denuded vessel can be evaluated accordingly. Therefore, L_p^E can be computed from *Eq. 5*. The denudation of ECs cannot exclude injury to the dorsal residual membrane of ECs on the basal membrane. Therefore, the residual membrane of ECs may affect the local permeability of the medial and adventitial layers. Other effects of the media-adventitia on permeability are potentially mediated by the vasoreactivity of vascular smooth muscle cells. Contraction or relaxation can change the dimension of the vessel (e.g., diameter and wall thickness) and

the cytoskeletal structure of the smooth muscle cell, which may alter the L_p of the media and adventitia. We measured L_p^{MA} at maximal vasoconstriction induced by 60 mM KCl and maximal vasodilation induced by Ca^{2+}-free PSS in denuded vessels (Fig. 5). We found that vasoreactive states did not significantly affect L_p^{MA}.

Endothelial barrier function consists of two parts: the EC layer and the glycocalyx lining on ECs. The glycocalyx consists of a highly hydrated mesh of membrane-associated proteoglycans, glycosaminoglycans, glycoproteins, and glycolipids (35, 36, 39) and is a very dynamic structure. The endothelial glycocalyx contributes as much as 60% of the hydraulic resistance of the capillary wall (39). The glycocalyx requires plasma proteins to maintain an optimal structure (13, 37). The removal of plasma proteins from the vascular perfusate results in increased L_p of the capillary wall (14, 16, 17). The role of the microvascular endothelial glycocalyx on filtration has been recognized in such diseases as diabetes, atherosclerosis, ischemia-reperfusion, and inflammation (5, 10, 30–33, 35, 48). Recently, the endothelial glycocalyx was visualized in carotid arteries of mice using two-photon microscopy (25). The functional role of the endothelial glycocalyx in conduit arteries (e.g., L_p) has been speculated as being similar to the microvasculature, and there are no direct data in large arteries. In the present study, we verified that the endothelial glycocalyx in femoral arteries of rats contributes over 50% to the L_p of the endothelial barrier (Fig. 4), which is consistent with the barrier function of water in capillaries. In a diabetic animal model, we found that the L_p of a femoral artery increased about twofold (from 6.8 to 12.5 $\times$ 10^{-7} cm·s^{-1}·cmH_2O^{-1}) in PSS-BSA but became similar (13.6 to 13.8 $\times$ 10^{-7} cm·s^{-1}·cmH_2O^{-1}) in PSS, which suggests that the endothelial glycocalyx in diabetic rats failed to provide hydraulic resistance, as it does in normal controls (Fig. 5). Treatment with protein-free perfusate (BSA-free PSS) provided neither specific nor quantitative assessment of glycocalyx components. Therefore, the barrier nature of the glycocalyx needs to be further studied using various enzymic digestions.

MLCK plays an important role in microvascular filtration by adjusting the adhesion junction of ECs. ML-7, a MLCK inhibitor, decreases filtration significantly by decreasing the gap of endothelial cell-cell adhesion junctions through interruption of the actomyosin contractile machinery (42, 51). Although the role of endothelial cell-cell adhesion junctions on the filtration of solutes (e.g., fluorescence-marked albumin) has been recognized in the microvasculature, the effect of endothelial cell-cell adhesion junctions on the L_p of conduit arteries was also significant, since measurements on the denuded endothelium showed a significant increase in the L_p of a conduit artery (Fig. 6). In femoral arteries of diabetic rats, L_p was slightly, but not statistically, decreased under experimental conditions (Fig. 6), which suggests that endothelial cell-cell adhesion junctions do not affect the endothelial L_p of conduit arteries, in contrast to the microvasculature.

In summary, the L_p of conduit arteries can be accurately and reproducibly measured using a new isovolumic method. This method is accurate, reproducible, and amenable to automation, as opposed to the particle-tracking method. The measurements showed that endothelial barrier filtration varies with diameter and wall thickness and is compromised in diabetic conduit arteries, likely, as the result of endothelial glycocalyx damage in hyperglycemia.

GRANTS

This research was supported in part by 3DT Holdings.

DISCLOSURES

No conflicts of interest, financial or otherwise, are declared by the author(s).

AUTHOR CONTRIBUTIONS

Author contributions: X.L., V.H.H., and G.S.K. conception and design of research; X.L. performed experiments; X.L., V.H.H., and G.S.K. analyzed data; X.L. and G.S.K. interpreted results of experiments; X.L. prepared figures; X.L. and G.S.K. drafted manuscript; X.L., V.H.H., and G.S.K. edited and revised manuscript; X.L., V.H.H., and G.S.K. approved final version of manuscript.

REFERENCES

1. **Baldwin AL, Wilson LM, Simon BR.** Effect of pressure on aortic hydraulic conductance. *Arterioscler Thromb* 12: 163–171, 1992.
2. **Becker BF, Chappell D, Jacob M.** Endothelial glycocalyx and coronary vascular permeability: the fringe benefit. *Basic Res Cardiol* 105: 687–701, 2010.
3. **Bingaman S, Huxley VH, Rumbaut RE.** Fluorescent dyes modify properties of proteins used in microvascular research. *Microcirculation* 10: 221–231, 2003.
4. **Bland JM, Altman DG.** Statistical methods for assessing agreement between two methods of clinical measurement. *The Lancet* 1: 307–310, 1986.
5. **Broekhuizen LN, Lemkes BA, Mooij HL, Meuwese MC, Verberne H, Holleman F, Schlingemann RO, Nieuwdorp M, Stroes ES, Vink H.** Effect of sulodexide on endothelial glycocalyx and vascular permeability in patients with type 2 diabetes mellitus. *Diabetologia* 53: 2646–2655, 2010.
6. **Chakraphan D, Sridulyakul P, Thipakorn B, Bunnag S, Huxley VH, Patumraj S.** Attenuation of endothelial dysfunction by exercise training in STZ-induced diabetic rats. *Clin Hemorheol Microcirc* 32: 217–226, 2005.
7. **Fry DL, Cornhill JF, Sharma H, Pap JM, Mitschelen J.** Uptake of low density lipoprotein, albumin, and water by deendothelialized in vitro minipig aorta. *Arteriosclerosis* 6: 475–490, 1986.
8. **Gouverneur M, Berg B, Nieuwdorp M, Stroes E, Vink H.** Vasculoprotective properties of the endothelial glycocalyx: effects of fluid shear stress. *J Intern Med* 259: 393–400, 2006.
9. **Kimura M, Dietrich HH, Huxley VH, Reichner DR, Dacey RG Jr.** Measurement of hydraulic conductivity in isolated arterioles of rat brain cortex. *Am J Physiol Heart Circ Physiol* 264: H1788–H1797, 1993.
10. **Kumar P, Shen Q, Pivetti CD, Lee ES, Wu MH, Yuan SY.** Molecular mechanisms of endothelial hyperpermeability: implications in inflammation. *Expert Rev Mol Med* 11: e19, 2009.
11. **Kumase F, Morizane Y, Mohri S, Takasu I, Ohtsuka A, Ohtsuki H.** Glycocalyx degradation in retinal and choroidal capillary endothelium in rats with diabetes and hypertension. *Acta Med Okayama* 64: 277–283, 2010.
12. **Huxley VH, Wang J.** Cardiovascular sex differences influencing microvascular exchange. *Cardiovasc Res* 87: 230–242, 2010.
13. **Huxley VH, Williams DA.** Role of a glycocalyx on coronary arteriole permeability to proteins: evidence from enzyme treatments. *Am J Physiol Heart Circ Physiol* 278: H1177–H1185, 2000.
14. **Huxley VH, Williams DA.** Models of microvascular barrier to proteins at luminal face of arteriole. *Am J Physiol Heart Circ Physiol* 278: H1177–H1185, 2000.
15. **Huxley VH, Curry FE, Powers MR, Thipakorn B.** Differential action of plasma and albumin on transcapillary exchange of anionic solute. *Am J Physiol Heart Circ Physiol* 264: H1428–H1437, 1993.
16. **Huxley VH, Meyer DJ Jr.** Capillary permeability: an albumin component attenuates active changes in Lp. *Am J Physiol Heart Circ Physiol* 259: H1357–H1364, 1990.
17. **Huxley VH, Curry FE.** Effect of superfusate albumin on single capillary hydraulic conductivity. *Am J Physiol Heart Circ Physiol* 252: H395–H401, 1987.

18. **Landis EM.** Micro-injection studies of capillary permeability. II. The relation between capillary pressure and the rate at which fluid passes through the walls of single capillaries. *Am J Physiol* 82: 217–238, 1917.
19. **Lemkes BA, Hermanides J, Devries JH, Holleman F, Meijers JC, Hoekstra JB.** Hyperglycemia: a prothrombotic factor? *J Thromb Haemost* 8: 1663–1669, 2010.
20. **Lennon FE, Singleton PA.** Hyaluronan regulation of vascular integrity. *Am J Cardiovasc Dis* 1: 200–213, 2011.
21. **Lu X, Kassab GS.** Assessment of endothelial function of large, medium, and small vessels: a unified myograph. *Am J Physiol Heart Circ Physiol* 300: H94–H100, 2011.
22. **Lu X, Guo X, Karathanasis SK, Zimmerman KM, Onyia JE, Peterson RG, Kassab GS.** Rosiglitazone reverses endothelial dysfunction but not remodeling of femoral artery in Zucker diabetic fatty rats. *Cardiovasc Diabetol* 9: 19, 2010.
23. **Lu X, Guo X, Linares C, Kassab GS.** A new method to denude the endothelium without damage to media: structural, functional, and biomechanical validation. *Am J Physiol Heart Circ Physiol* 286: H1889–H1894, 2004.
24. **Mason JC, Michel CC, Shaw TC, Tooke JE.** The measurement of the filtration coefficienct of the walls of single frog mesenteric capillaries using the movement of red cells. *J Physiol Suppl* 218: 26P–27P, 1971.
25. **Megens RT, Reitsma S, Schiffers PH, Hilgers RH, De Mey JG, Slaaf DW, oude Egbrink MG, van Zandvoort MA.** Two-photon microscopy of vital murine elastic and muscular arteries. Combined structural and functional imaging with subcellular resolution. *J Vasc Res* 44: 87–98, 2007.
26. **Michel CC, Curry FR.** Glycocalyx volume: a critical review of tracer dilution methods for its measurement. *Microcirculation* 16: 213–219, 2009. Erratum in: *Microcirculation* 16: 544–546, 2009.
27. **Michel CC, Curry FE.** Microvascular permeability. *Physiol Rev* 79: 703–761, 1999.
28. **Michel CC, Mason JC, Curry FE, Tooke JE, Hunter PJ.** A development of the Landis technique for measuring the filtration coefficient of individual capillaries in the frog mesentery. *Q J Exp Physiol Cogn Med Sci* 59: 283–309, 1974.
29. **Nassimizadeh M, Ashrafian H, Drury NE, Howell NJ, Digby J, Pagano D, Frenneaux MP, Born GV.** Reduced negative surface charge on arterial endothelium explains accelerated atherosclerosis in type 2 diabetic patients. *Diab Vasc Dis Res* 7: 213–215, 2010.
30. **Nieuwdorp M, Holleman F, de Groot E, Vink H, Gort J, Kontush A, Chapman MJ, Hutten BA, Brouwer CB, Hoekstra JB, Kastelein JJ, Stroes ES.** Perturbation of hyaluronan metabolism predisposes patients with type 1 diabetes mellitus to atherosclerosis. *Diabetologia* 50: 1288–1293, 2007.
31. **Nieuwdorp M, Mooij HL, Kroon J, Atasever B, Spaan JA, Ince C, Holleman F, Diamant M, Heine RJ, Hoekstra JB, Kastelein JJ, Stroes ES, Vink H.** Endothelial glycocalyx damage coincides with microalbuminuria in type 1 diabetes. *Diabetes* 55: 1127–1132, 2006.
32. **Nieuwdorp M, van Haeften TW, Gouverneur MC, Mooij HL, van Lieshout MH, Levi M, Meijers JC, Holleman F, Hoekstra JB, Vink H, Kastelein JJ, Stroes ES.** Loss of endothelial glycocalyx during acute hyperglycemia coincides with endothelial dysfunction and coagulation activation in vivo. *Diabetes* 55: 480–486, 2006.
33. **Noble MI, Drake-Holland AJ, Vink H.** Hypothesis: arterial glycocalyx dysfunction is the first step in the atherothrombotic process. *QJM* 101: 513–518, 2008.
34. **Osterloh K, Ewert U, Pries AR.** Interaction of albumin with the endothelial cell surface. *Am J Physiol Heart Circ Physiol* 283: H398–H405, 2002.
35. **Perrin RM, Harper SJ, Bates DO.** A role for the endothelial glycocalyx in regulating microvascular permeability in diabetes mellitus. *Cell Biochem Biophys* 49: 65–72, 2007.
36. **Perrin RM, Harper SJ, Corrall R, Bates DO.** Hyperglycemia stimulates a sustained increase inhydraulic conductivity in vivo without any change in reflection coefficient. *Microcirculation* 14: 683–696, 2007.
37. **Pries AR, Secomb TW, Gaehtgens P.** The endothelial surface layer. *Pflugers Arch* 440: 653–666, 2000.
38. **Rana JS, Nieuwdorp M, Jukema JW, Kastelein JJ.** Cardiovascular metabolic syndrome - an interplay of, obesity, inflammation, diabetes and coronary heart disease. *Diabetes Obes Metab* 9: 218–232, 2007.
39. **Reitsma S, Slaaf DW, Vink H, van Zandvoort MA, oude Egbrink MG.** The endothelial glycocalyx: composition, functions, and visualization. *Pflugers Arch* 454: 345–359, 2007.
40. **Rumbaut RE, McKay MK, Huxley VH.** Capillary hydraulic conductivity is decreased by nitric oxide synthase inhibition. *Am J Physiol Heart Circ Physiol* 268: H1856–H1861, 1995.
41. **Salmon AH, Satchell SC.** Endothelial glycocalyx dysfunction in disease: albuminuria and increased microvascular permeability. *J Pathol* 226: 562–574, 2012.
42. **Shen Q, Rigor RR, Pivetti CD, Wu MH, Yuan SY.** Myosin light chain kinase in microvascular endothelial barrier function. *Cardiovasc Res* 87: 272–280, 2010.
43. **Singh A, Fridén V, Dasgupta I, Foster RR, Welsh GI, Tooke JE, Haraldsson B, Mathieson PW, Satchell SC.** High glucose causes dysfunction of the human glomerular endothelial glycocalyx. *Am J Physiol Renal Physiol* 300: F40–F48, 2011.
44. Starling (1896a) EH. On the absorption of fluids from connective tissue spaces. *J Physiol* 19: 312–326, 1896.
45. **Tarbell JM, Lever MJ, Caro CG.** The effect of varying albumin concentration of the hydraulic conductivity of the rabbit common carotid artery. *Microvasc Res* 35: 204–220, 1988.
46. **van den Berg BM, Vink H, Spaan JA.** The endothelial glycocalyx protects against myocardial edema. *Circ Res* 92: 592–594, 2003.
47. **Vandenbroucke E, Mehta D, Minshall R, Malik AB.** Regulation of endothelial junctional permeability. *Ann NY Acad Sci* 1123: 134–145, 2008.
48. **van Golen RF, van Gulik TM, Heger M.** Mechanistic overview of reactive species-induced degradation of the endothelial glycocalyx during hepatic ischemia/reperfusion injury. *Free Radic Biol Med* 52: 1382–1402, 2012.
49. **Vargas CB, Vargas FF, Pribyl JG, Blackshear PL.** Hydraulic conductivity of the endothelial and outer layers of the rabbit aorta. *Am J Physiol Heart Circ Physiol* 236: H53–H60, 1979.
50. **Wheeler-Jones CP, Farrar CE, Pitsillides AA.** Targeting hyaluronan of the endothelial glycocalyx for therapeutic intervention. *Curr Opin Investig Drugs* 11: 997–1006, 2010.
51. **Yuan Y, Huang Q, Wu HM.** Myosin light chain phosphorylation: modulation of basal and agonist-stimulated venular permeability. *Am J Physiol Heart Circ Physiol* 272: H1437–H1443, 1997.
52. **Zuurbier CJ, Demirci C, Koeman A, Vink H, Ince C.** Short-term hyperglycemia increases endothelial glycocalyx permeability and acutely decreases lineal density of capillaries with flowing red blood cells. *J Appl Physiol* 99: 1471–1476, 2005.